Letter

Floquet Weyl states at one-photon resonance: An origin of nonperturbative optical responses in three-dimensional materials

Yoshua Hirai [1], Shun Okumura [2], Naotaka Yoshikawa [1], Takashi Oka [3], and Ryo Shimano [1,4]

[1] *Department of Physics, The University of Tokyo, Hongo, Tokyo 113-0033, Japan*
[2] *Department of Applied Physics, The University of Tokyo, Hongo, Tokyo 113-8656, Japan*
[3] *Institute for Solid State Physics, The University of Tokyo, Kashiwa, Chiba 277-8581, Japan*
[4] *Cryogenic Research Center, The University of Tokyo, Yayoi, Tokyo 113-0032, Japan*

(Received 23 October 2023; accepted 10 January 2024; published 9 February 2024)

Electrons driven coherently by laser light can exhibit nonperturbative geometric effects. Drastic deformation and gap openings of the electrons' Floquet bands occur at one-photon resonances since the electron and hole bands hybridize through their replicas at the lowest-order photon exchange. We study the evolution of Floquet bands in three-dimensional (3D) materials driven by circularly polarized light (CPL) using the Dirac model. We find that the light-induced gap closes at a select few points in the momentum space where Floquet Weyl points are formed. The Weyl points are protected by their monopole charge and can merge, separate, or pair annihilate depending on the anisotropy of electrons and the ellipticity of the incident light. In isotropic 3D Dirac electrons driven by CPL, the Weyl points merge to form Floquet double-Weyl points with topological charge ± 2. Our results reveal a universal aspect of light-matter interactions in 3D quantum materials and open a route towards controllable versatile electromagnetic responses associated with light-induced Floquet Weyl states.

DOI: 10.1103/PhysRevResearch.6.L012027

Introduction. Exploring the nonthermal control of quantum materials using coherent and intensive laser light is an active field of research [1–4]. It is a challenge to understand the nonequilibrium dynamics of driven electrons due to the concurrent occurrence of multiple nonlinear phenomena [5–10]. When electrons are driven time-periodically by laser fields, they become photodressed and are described by Floquet states [4,11–13]. Experimental investigations in two-dimensional systems have revealed the critical role of Floquet bands and the modification of their gaps in understanding the optical response in the nonperturbative regime [5–7]. Notably, the Berry curvature (BC) associated with the Floquet states [8] can result in a light-induced anomalous Hall response [6]. Currently, research is expanding into the study of the light-induced anomalous Hall effect in three-dimensional (3D) quantum materials [14–16], motivated partly by the hypothesis of Floquet Weyl points. This hypothesis posits that circularly polarized light (CPL) effectively generates a light-induced chiral gauge field, thereby converting 3D Dirac electrons into Weyl electrons with broken time-reversal symmetry [17–20].

However, recent studies on the light-induced anomalous Hall effect in bismuth suggest that the light-induced chiral gauge field scenario does not fully account for all the observed phenomena [14]. Bismuth features a small gap at the Dirac point, and the light-induced chiral gauge field can only barely close this gap and facilitate the transformation into Weyl electrons. This realization compels us to search for alternative sources of BC, prompting a more detailed reexamination of Floquet bands.

In this Letter, we demonstrate that the emergence of Weyl states is an even more general feature of 3D Dirac electrons when they are resonantly driven, independent of the mass gap size and the driving field strength. By analyzing CPL-driven 3D Dirac electrons based on Floquet theory, we find pairs of Weyl states to appear at the one-photon resonant positions in the quasienergy spectrum (i.e., at the Floquet zone boundaries). These resonant Weyl states carry the topological charge of ± 2 for strictly isotropic 3D Dirac electrons, which are twice that of ordinary Weyl points, and hence we call them Floquet double-Weyl points (FDWPs). We systematically investigate the effects of the Dirac mass, anisotropy of Dirac electrons, and ellipticity of the driving fields. We find that the double-Weyl state is sensitive to such conditions and may split into ordinary Weyl points, but their existence appears robust due to topological protection. Given that the Dirac Hamiltonian expresses a wide range of materials with spin-orbit coupling [21], our results reveal a general and so-far-overlooked topological aspect of the light-matter interaction.

Floquet analysis of isotropic 3D Dirac electrons. We denote the single-body 3D Dirac Hamiltonian as

$$\mathcal{H}_{\mathrm{Dirac}}(\mathbf{p}) = \gamma^0\left(\Delta + v_x\gamma^x p_x + v_y\gamma^y p_y + v_z\gamma^z p_z\right), \qquad (1)$$

where $\mathbf{p}$, Δ, and $\mathbf{v}$ are the electron momentum, mass term, and the velocity matrix element, respectively. γ^μ are the gamma matrices which satisfy $\{\gamma^\mu, \gamma^\nu\} = 2\eta^{\mu\nu}$. We will temporarily limit the argument to isotropic 3D Dirac electrons, which assumes $v_x = v_y = v_z$. The coupling between the Dirac

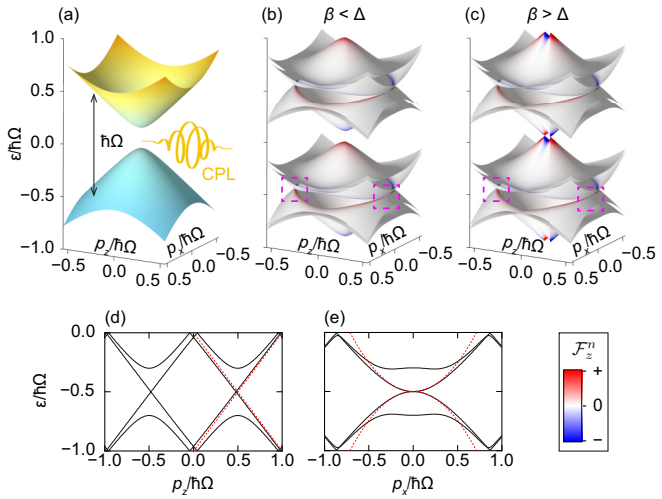

FIG. 1. (a) Massive 3D Dirac electrons driven by CPL and (b) the equivalent Floquet quasienergy band structure. The chiral gauge field strength β is smaller than the mass term Δ. (c) The Floquet quasienergy band structure for massless Dirac electrons. The color scale in (b) and (c) indicates the z component of BC. Cuts containing the node near $p_z = \Omega/2$ are displayed in (d) and (e) for the z and x directions, respectively (solid lines). The red dashed lines in (d) and (e) show the quasienergy dispersions of $\mathcal{H}^+_{\rm eff}$ [see Eq. (4)].

electrons and optical driving fields is implemented by minimum coupling $\mathbf{p} \to \mathbf{p} + \mathbf{A}(t)$, where $\mathbf{A}(t)$ is the time-dependent vector potential (we have chosen the unit system so that $e = \hbar = 1$). If the optical driving field is CPL propagating in the z direction, the explicit form of $\mathbf{A}(t)$ is given as $\mathbf{A}(t) = (A\cos\Omega t, A\sin\Omega t, 0)$, where Ω is the angular frequency of the CPL. This leads to a time-dependent Hamiltonian

$$\mathcal{H}(\mathbf{p}, t) = \gamma^0\Delta + \gamma^0\boldsymbol{\gamma}\cdot\mathbf{p} + \gamma^0\boldsymbol{\gamma}\cdot\mathbf{A}(t), \tag{2}$$

which possesses the time periodicity $\mathcal{H}(\mathbf{p}, t+T) = \mathcal{H}(\mathbf{p}, t)$, where $T = 2\pi/\Omega$ is the period of the optical drive. This time-periodic nature of the Hamiltonian enables the application of Floquet theory [4,11,12].

The building blocks of Floquet theory are the Fourier transforms of the time-periodic Hamiltonian, defined by $\mathcal{H}(\mathbf{p}, t) = \sum_m e^{-im\Omega t}\mathcal{H}^m(\mathbf{p})$. Floquet theory translates the original time-dependent finite-dimension eigenvalue problem into a time-independent infinite-dimension eigenvalue problem, with the Hamiltonian now being the Floquet Hamiltonian $\mathcal{H}_{\rm F}$ defined as

$$\mathcal{H}_{\rm F} = \begin{pmatrix} \ddots & \ddots & \ddots & \ddots & \ddots \\ \ddots & \mathcal{H}^0+\Omega & \mathcal{H}^1 & \mathcal{H}^2 & \ddots \\ \ddots & \mathcal{H}^{-1} & \mathcal{H}^0 & \mathcal{H}^1 & \ddots \\ \ddots & \mathcal{H}^{-2} & \mathcal{H}^{-1} & \mathcal{H}^0-\Omega & \ddots \\ \ddots & \ddots & \ddots & \ddots & \ddots \end{pmatrix}. \tag{3}$$

In Fig. 1(b), we display the Floquet quasienergy band structure calculated based on Eq. (3) for massive ($\Delta > 0$) Dirac electrons alongside the band structure of its nondriven counterpart [Fig. 1(a)]. The complex band structure can be understood as replicas of the original Dirac band overlaid onto each other with the energy interval of Ω, followed by gap openings where the replica bands intersect. The overall quasienergy band structure is periodic with the period of Ω and the minimal unit of $-\Omega/2 \leqslant \varepsilon \leqslant \Omega/2$, which is in accordance with Floquet theory. For comparison, we have also displayed the Floquet quasienergy band structure for massless ($\Delta = 0$) Dirac electrons in Fig. 1(c). Near the original Dirac point, one can see a pair of linear dispersions accompanied by the concentration of BC. These are the Floquet Weyl states at zero energy [17–20], which arise when the CPL-induced chiral gauge field strength $\beta = A^2/\Omega$ is greater than the mass term Δ. This condition is always satisfied for massless Dirac electrons [Fig. 1(c)] but not necessarily satisfied for massive Dirac electrons [Fig. 1(b)].

Floquet Weyl states at one-photon resonance. In the Floquet spectrum [Figs. 1(b) and 1(c)], we notice that a gap is formed in a ring-shaped region at the Floquet zone boundaries $\varepsilon = \pm\Omega/2$ and BC emerges along it. This gap is a 3D analog of the topological gap discussed in Ref. [9] for a two-dimensional (2D) system, and its maximum size is given by $2A$ for $\Delta = 0$. This gap is formed by hybridization between the electron and hole bands by a one-photon absorption process. Unlike the 2D case, the gap closes at two points in momentum space, forming a pair of FDWPs. They show linear dispersions in the z direction [Fig. 1(d), solid lines] while showing a quadratic band touching in the x and y direction [Fig. 1(e), solid lines]. Surprisingly, the FDWPs at one-photon resonance are present even in the massive case without any threshold field strength, which is in contrast to the Floquet Weyl points at zero energy that emerge only for strong fields realizing $\beta > \Delta$. The characterization of the Floquet Weyl states at one-photon resonances will be the main content of this Letter.

Effective model and Berry curvature. To gain insight into the FDWPs at one-photon resonance, we limit ourselves to the massless case and construct an effective two-band model around $\mathbf{p} = (0, 0, \pm\Omega/2)$ [22]. The resultant two-by-two effective Hamiltonian accounting for the node at $\mathbf{p} = (0, 0, \pm\Omega/2)$ is

$$\mathcal{H}^{\pm}_{\rm eff} = -\frac{\Omega}{2} \mp k_z\sigma_z - \frac{1}{A^2+\Omega^2}\begin{pmatrix} \Omega|k|^2 & \mp Ak^2 \\ \mp Ak^{*2} & -\Omega|k|^2 \end{pmatrix}, \tag{4}$$

where $\mathbf{k}$ is the momentum defined from each node and $k = k_x + ik_y$. The band structure based on $\mathcal{H}^+_{\rm eff}$ is displayed in Figs. 1(d) and 1(e) as red dashed lines. The effective Hamiltonian faithfully reproduces the Floquet band structure around the gap closure.

The two-by-two form of the effective Hamiltonian enables insightful calculations regarding the topological nature of these Floquet Weyl points. In particular, the BC distribution can be calculated analytically as [23]

$$\mathcal{F}^{\pm}_{x,y} = \mp\frac{k_{x,y}}{(E^{\pm})^3}\frac{A^2(k_x^2+k_y^2)}{(A^2+\Omega^2)^2}, \tag{5}$$

$$\mathcal{F}^{\pm}_{z} = \mp\frac{2k_z}{(E^{\pm})^3}\frac{A^2(k_x^2+k_y^2)}{(A^2+\Omega^2)^2} \tag{6}$$

where $-\Omega/2 + E^{\pm}$ is the larger eigenenergy of $\mathcal{H}^{\pm}_{\rm eff}$. The BC and normalized BC are displayed in Figs. 2(a) and 2(b), respectively. The node under discussion acts as a source/sink of BC, which means the node is topological. The associated

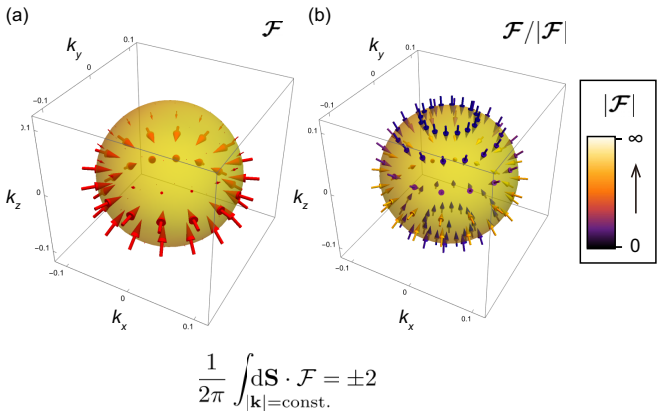

FIG. 2. (a) BC and (b) normalized BC distribution based on $\mathcal{H}^{+}_{\text{eff}}$. The node represented by $\mathcal{H}^{+}_{\text{eff}}$ acts as a sink of BC, and the associated topological charge is $\chi = -2$.

topological charge is ± 2, which is defined by

$$\chi = \frac{1}{2\pi}\int_{\Sigma} d\mathbf{S}\cdot\mathcal{F}, \tag{7}$$

where Σ is a closed surface surrounding one of the topological nodes. This confirms that the node is what could be called a FDWP. It is worth noting that though double-Weyl semimetals have been theoretically debated [24–26] and also predicted for some specific materials in equilibrium [27–29], they have not yet been experimentally realized in solid-state systems. Our results provide a way of realizing double-Weyl semimetal states through Floquet engineering.

Effect of anisotropy and ellipticity. We further consider anisotropic 3D Dirac electrons under the irradiation of elliptically polarized light (EPL). In fact, we can show that introducing finite ellipticity is equivalent to introducing anisotropy to the 3D Dirac electrons while keeping the light circularly polarized [22]. Therefore, we focus on CPL-driven anisotropic 3D Dirac electrons. The degree of anisotropy is quantified by $v_{-} = (v_x - v_y)/2$.

Figures 3(a)–3(c) show the evolution of the nodal structure under finite CPL amplitude and finite anisotropy. The nodal sphere [Fig. 3(a)] that is formed due to the intersection between the hole band and the $\hbar\Omega$-shifted electron band gaps out by driving it with finite CPL amplitude [Fig. 3(b)], except for the two FDWPs. Introducing finite anisotropy splits each FDWP into two separate nodes [Fig. 3(c)]. A cut of the quasienergy band structure along the z direction and the density of states (DoS) are shown in Figs. 3(d) and 3(e). The DoS distribution for the isotropic case shows a linear behavior against the quasienergy around the FDWPs and shows additional peaks near the gapped-out bands. After introducing finite anisotropy, kinks appear in the DoS distribution due to additional critical points where the FDWPs used to be. The most important feature, however, is the transition from the linear to the quadratic behavior to the quasienergy at the nodal position. This quadratic behavior of the quasienergy indicates that the four nodes depicted in Fig. 3(c) possess linear dispersions [22], which suggest that they are all normal Weyl points.

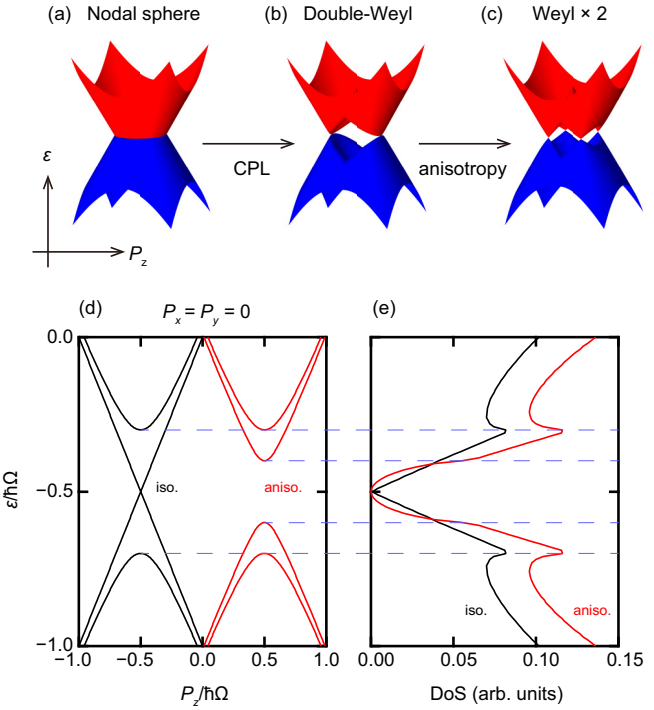

FIG. 3. (a)–(c) The evolution of quasienergy band structure under finite CPL amplitude and finite anisotropy. (d) Cut of the quasienergy band structure in the z direction. The $P_z > 0$ ($P_z < 0$) region shows the results for anisotropic (isotropic) 3D Dirac electrons. (e) DoS distribution for the isotropic and anisotropic case. $A = 0.2$ and $v_{-} = 0.0, 0.5$ are used to obtain (d) and (e).

To further confirm the split from FDWPs into two normal Weyl points, we have calculated the BC distribution for both the isotropic and the anisotropic cases, which are shown in Figs. 4(a) and 4(b) (we have redefined the momentum as $P_i = v_i p_i$). The BC near the four nodal positions in Fig. 4(b) shows diverging structures just as those near the FDWPs in Fig. 4(a), which indicates that the nodes carry nonzero topological charges. The fact that the nodes originate from the split of FDWPs, the linear dispersion around each node, and the diverging BC distribution indicate that the four nodes that emerge in anisotropic 3D Dirac electrons are all normal Weyl points.

Having established the topology associated with the nodal structure, we show the Weyl point positions for various degrees of anisotropy (v_{-}) and CPL amplitude (A) in Fig. 4(c). We have only shown the results for $v_{-} > 0$ in Fig. 4(a), but identical results hold for $v_{-} < 0$ as well, the only difference being that for the latter case nodes only appear in the y-z plane instead of the x-z plane. The shift of the Weyl point position due to increasing CPL amplitude is a feature not observed for FDWPs. Note that the CPL amplitude only moves the Weyl points in the x or y direction and not the z direction.

As we have already mentioned, the effect of EPL driving can be absorbed into the anisotropy of the Dirac electrons, which leads to several interesting implications. First, one can effectively tune the anisotropy of Dirac electrons by varying the ellipticity. This is advantageous for practical experiments since the latter is easier to control than the former during

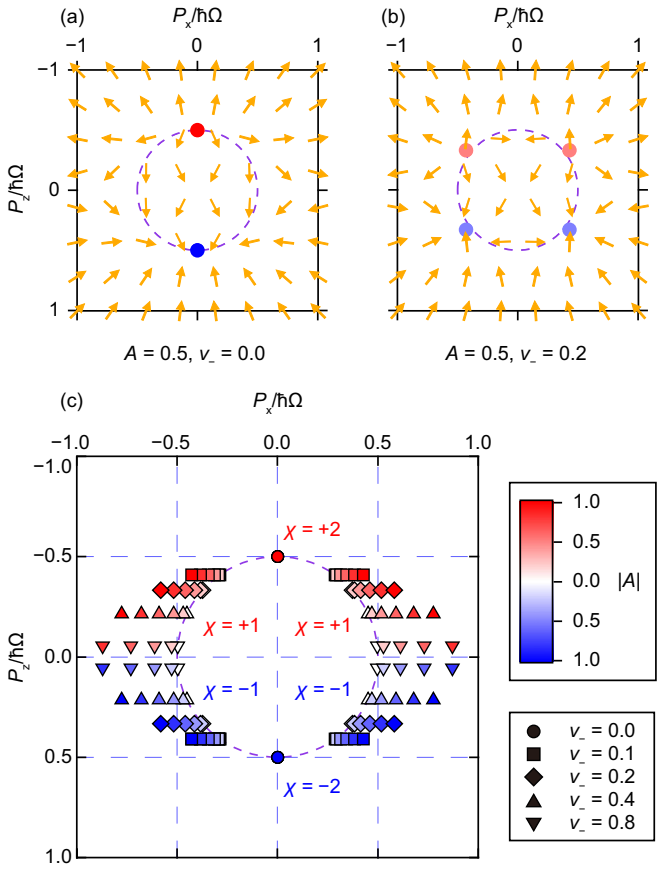

FIG. 4. (a), (b) The BC distribution for CPL-driven isotropic/anisotropic 3D Dirac electrons. The diverging structure of BC indicates that the nodes all have nonzero topological charges. (c) Node positions at one-photon resonances for CPL-driven anisotropic 3D Dirac electrons. The degree of anisotropy (v_-) and CPL amplitude (A) are represented by the symbol shape and color scale, respectively [$v_+ = (v_x + v_y)/2$ is set to unity]. The red and blue colors of the node indicate the sign of the associated topological charge χ.

optical measurements. Second, one can adjust the ellipticity of EPL so that the Floquet system is equivalent to isotropic Dirac electrons driven by CPL, even for anisotropic Dirac electrons. This is important since the isotropic nature is crucial for the emergence of FDWPs, though it is rare in realistic materials [21,30–33]. Third, this theoretical framework provides continuity between CPL-driven and linearly polarized light-driven Dirac electrons. The only difference between them is the ellipticity, and the linearly polarized light-driven state can be seen as CPL-driven Dirac electrons that are infinitely anisotropic. Under this condition, the four topological nodes reside at $P_z = 0$, resulting in annihilation and possibly a gap-out.

Experimental realization. Finally, we would like to discuss the possibility of experimental realizations of this double-Weyl state. Figure 3(e) indicates a finite quasienergy window where the band structure is well described by FDWP pairs, which is the region between the two peaks in the DoS. The size of the energy window is $2vA$ for isotropic 3D Dirac electrons, where $v_x = v_y = v_z = v$ [we have assumed $v = 1$ for the construction of Eq. (4)].

As a typical example of a realistic material hosting 3D Dirac electrons, we consider the group-V semimetal bismuth. The Dirac electrons in bismuth are extremely anisotropic ($v_x = v_z = 8.1 \times 10^5$ m/s and $v_y = 6.6 \times 10^4$ m/s) [30], which requires $|A_y|/|A_x| \simeq 12$ for the FDWPs to form. Using the redefined velocity for this ellipticity, $v = 0.93 \times 10^5$ m/s, and typical electric field strengths and midinfrared photon energies of $E = 0.7$ MV/cm and $\hbar\Omega = 0.3$ eV, respectively, we obtain the quasienergy window size of $2vE/\Omega \simeq 29$ meV, which is comparable to the energy corresponding to room temperature (26 meV). Additional caution is necessary when considering realistic materials, however, since it is typical for such materials to have multiple electron (or hole) pockets that host Dirac electrons, which orient themselves in different directions.

How the emergence of FDWPs can be experimentally demonstrated is a fascinating issue. Aside from the direct observation of Floquet-Bloch quasienergy bands, e.g., by angle-resolved photoemission spectroscopy measurements, conventional signatures of Weyl semimetals such as the intrinsic anomalous Hall effect, negative magnetoresistance by chiral anomaly, and emergence of Fermi-arc surface states may provide fingerprints of the Floquet double-Weyl state. At the same time, we also point out that further theoretical investigation is necessary to determine how the above phenomena known for equilibrium Weyl semimetals manifest themselves in nonequilibrium cases. This is because of the nonequilibrium and nonuniform nature of the occupancy distribution, which depends on the details of dissipation mechanisms within the system [34,35]. Other nonlinear optical effects including high-harmonic generation, shift currents, and injection currents are also promising probes for experimentally demonstrating the emergence of FDWPs [36,37].

Conclusion. In this Letter, we examined 3D Dirac electrons driven by resonant laser light and analyzed their topological properties. Two pairs of Weyl points emerge at the Floquet zone boundaries due to one-photon resonance and merge into one pair of FDWPs depending on the anisotropy and ellipticity. The emergence of these Weyl points is an extremely general and universal feature and happens as long as the following three conditions are met: The driving field is one-photon resonant with the Dirac electrons, the Dirac electrons are 3D, and the driving field breaks time-reversal symmetry. The results also do not depend on the size of the Dirac mass [22] nor do they rely on the high-frequency expansion, which make our results applicable to and feasible to realize for a wide variation of materials with spin-orbit coupling [21]. Our results reveal a link between Weyl physics and light-matter interactions, as well as open a route towards highly controllable electromagnetic responses associated with the light-induced Weyl states.

Acknowledgments. We acknowledge T. Morimoto, M. Schüler, S. A. Sato, M. Kawaguchi, and M. Hayashi for their fruitful discussions. This work was supported by JST CREST (Grant No. JPMJCR19T3), Japan. Y.H. was supported by Grant-in-Aid for JSPS Research Fellows (Grant No. 21J20873). S.O. was supported by JSPS KAKENHI (Grant No. JP22K13998).

Y.H. and S.O. contributed equally to this work.

[1] D. N. Basov, R. D. Averitt, and D. Hsieh, Towards properties on demand in quantum materials, Nat. Mater. **16**, 1077 (2017).

[2] A. de la Torre, D. M. Kennes, M. Claassen, S. Gerber, J. W. McIver, and M. A. Sentef, *Colloquium*: Nonthermal pathways to ultrafast control in quantum materials, Rev. Mod. Phys. **93**, 041002 (2021).

[3] J. Orenstein, Ultrafast spectroscopy of quantum materials, Phys. Today **65** (9), 44 (2012).

[4] T. Oka and S. Kitamura, Floquet engineering of quantum materials, Annu. Rev. Condens. Matter Phys. **10**, 387 (2019).

[5] Y. H. Wang, H. Steinberg, P. Jarillo-Herrero, and N. Gedik, Observation of Floquet-Bloch states on the surface of a topological insulator, Science **342**, 453 (2013).

[6] J. W. McIver, B. Schulte, F. U. Stein, T. Matsuyama, G. Jotzu, G. Meier, and A. Cavalleri, Light-induced anomalous Hall effect in graphene, Nat. Phys. **16**, 38 (2020).

[7] S. Ito, M. Schüler, M. Meierhofer, S. Schlauderer, J. Freudenstein, J. Reimann, D. Afanasiev, K. A. Kokh, O. E. Tereshchenko, J. Güdde, M. A. Sentef, U. Höfer, and R. Huber, Build-up and dephasing of Floquet–Bloch bands on subcycle timescales, Nature (London) **616**, 696 (2023).

[8] T. Oka and H. Aoki, Photovoltaic Hall effect in graphene, Phys. Rev. B **79**, 081406(R) (2009).

[9] N. H. Lindner, G. Refael, and V. Galitski, Floquet topological insulator in semiconductor quantum wells, Nat. Phys. **7**, 490 (2011).

[10] S. A. Sato, J. W. McIver, M. Nuske, P. Tang, G. Jotzu, B. Schulte, H. Hübener, U. De Giovannini, L. Mathey, M. A. Sentef, A. Cavalleri, and A. Rubio, Microscopic theory for the light-induced anomalous Hall effect in graphene, Phys. Rev. B **99**, 214302 (2019).

[11] U. D. Giovannini and H. Hübener, Floquet analysis of excitations in materials, J. Phys. Mater. **3**, 012001 (2019).

[12] M. S. Rudner and N. H. Lindner, Band structure engineering and non-equilibrium dynamics in Floquet topological insulators, Nat. Rev. Phys. **2**, 229 (2020).

[13] A. Eckardt, *Colloquium*: Atomic quantum gases in periodically driven optical lattices, Rev. Mod. Phys. **89**, 011004 (2017).

[14] Y. Hirai, N. Yoshikawa, M. Kawaguchi, M. Hayashi, S. Okumura, T. Oka, and R. Shimano, Anomalous Hall effect of light-driven three-dimensional Dirac electrons in bismuth, arXiv:2301.06072.

[15] N. Yoshikawa, Y. Hirai, K. Ogawa, S. Okumura, J. Fujiwara, Kohei Ikeda, T. Koretsune, A. Arita, Ryotaro Mitra, A. Tsukazaki, T. Oka, and R. Shimano, Light-induced chiral gauge field in a massive 3D Dirac electron system, arXiv:2209.11932.

[16] Y. Murotani, N. Kanda, T. Fujimoto, T. Matsuda, M. Goyal, J. Yoshinobu, Y. Kobayashi, T. Oka, S. Stemmer, and R. Matsunaga, Disentangling the competing mechanisms of light-induced anomalous Hall conductivity in three-dimensional Dirac semimetal, Phys. Rev. Lett. **131**, 096901 (2023).

[17] R. Wang, B. Wang, R. Shen, L. Sheng, and D. Y. Xing, Floquet Weyl semimetal induced by off-resonant light, Europhys. Lett. **105**, 17004 (2014).

[18] S. Ebihara, K. Fukushima, and T. Oka, Chiral pumping effect induced by rotating electric fields, Phys. Rev. B **93**, 155107 (2016).

[19] H. Hübener, M. A. Sentef, U. De Giovannini, A. F. Kemper, and A. Rubio, Creating stable Floquet-Weyl semimetals by laser-driving of 3D Dirac materials, Nat. Commun. **8**, 13940 (2017).

[20] L. Bucciantini, S. Roy, S. Kitamura, and T. Oka, Emergent Weyl nodes and Fermi arcs in a Floquet Weyl semimetal, Phys. Rev. B **96**, 041126(R) (2017).

[21] Y. Fuseya, M. Ogata, and H. Fukuyama, Transport properties and diamagnetism of Dirac electrons in bismuth, J. Phys. Soc. Jpn. **84**, 012001 (2015).

[22] See Supplemental Material at http://link.aps.org/supplemental/10.1103/PhysRevResearch.6.L012027 for a detailed derivation of the effective Hamiltonian, effects of anisotropy and ellipticity, the density of states of Weyl and double-Weyl semimetals, and the effects of finite mass.

[23] Y. Suzumura and A. Kobayashi, Berry curvature of the Dirac particle in α-(BEDT-TTF)$_2$I$_3$, J. Phys. Soc. Jpn. **80**, 104701 (2011).

[24] C. Fang, M. J. Gilbert, X. Dai, and B. A. Bernevig, Multi-Weyl topological semimetals stabilized by point group symmetry, Phys. Rev. Lett. **108**, 266802 (2012).

[25] Z.-M. Huang, J. Zhou, and S.-Q. Shen, Topological responses from chiral anomaly in multi-Weyl semimetals, Phys. Rev. B **96**, 085201 (2017).

[26] R. M. A. Dantas, F. Peña-Benitez, B. Roy, and P. Surówka, Non-Abelian anomalies in multi-Weyl semimetals, Phys. Rev. Res. **2**, 013007 (2020).

[27] S.-M. Huang, S.-Y. Xu, I. Belopolski, C.-C. Lee, G. Chang, T.-R. Chang, B. Wang, N. Alidoust, G. Bian, M. Neupane, D. Sanchez, H. Zheng, H.-T. Jeng, A. Bansil, T. Neupert, H. Lin, and M. Z. Hasan, New type of Weyl semimetal with quadratic double Weyl fermions, Proc. Natl. Acad. Sci. USA **113**, 1180 (2016).

[28] B. Singh, G. Chang, T. R. Chang, S. M. Huang, C. Su, M. C. Lin, H. Lin, and A. Bansil, Tunable double-Weyl fermion semimetal state in the SrSi$_2$ materials class, Sci. Rep. **8**, 10540 (2018).

[29] N. Heinsdorf, M. H. Christensen, M. Iraola, S. S. Zhang, F. Yang, T. Birol, C. D. Batista, R. Valentí, and R. M. Fernandes, Prediction of double-Weyl points in the iron-based superconductor CaKFe$_4$As$_4$, Phys. Rev. B **104**, 075101 (2021).

[30] J. Ruhman and P. A. Lee, Pairing from dynamically screened Coulomb repulsion in bismuth, Phys. Rev. B **96**, 235107 (2017).

[31] Z. K. Liu, B. Zhou, Y. Zhang, Z. J. Wang, H. M. Weng, D. Prabhakaran, S.-K. Mo, Z. X. Shen, Z. Fang, X. Dai, Z. Hussain, and Y. L. Chen, Discovery of a three-dimensional topological Dirac semimetal, Na$_3$Bi, Science **343**, 864 (2014).

[32] I. Crassee, R. Sankar, W.-L. Lee, A. Akrap, and M. Orlita, 3D Dirac semimetal Cd$_3$As$_2$: A review of material properties, Phys. Rev. Mater. **2**, 120302 (2018).

[33] F. Le Mardelé, J. Wyzula, I. Mohelsky, S. Nasrallah, M. Loh, S. Ben David, O. Toledano, D. Tolj, M. Novak, G. Eguchi, S. Paschen, N. Barišić, J. Chen, A. Kimura, M. Orlita, Z. Rukelj, A. Akrap, and D. Santos-Cottin, Evidence for three-dimensional Dirac conical bands in TlBiSSe by optical and magneto-optical spectroscopy, Phys. Rev. B **107**, L241101 (2023).

[34] H. Dehghani, T. Oka, and A. Mitra, Dissipative Floquet topological systems, Phys. Rev. B **90**, 195429 (2014).

[35] M. Schüler, U. De Giovannini, H. Hübener, A. Rubio, M. A. Sentef, T. P. Devereaux, and P. Werner, How circular dichroism in time- and angle-resolved photoemission can be used to spectroscopically detect transient topological states in graphene, Phys. Rev. X **10**, 041013 (2020).

[36] T. Morimoto and N. Nagaosa, Topological nature of nonlinear optical effects in solids, Sci. Adv. **2**, e1501524 (2016).

[37] T. Morimoto, S. Kitamura, and N. Nagaosa, Geometric aspects of nonlinear and nonequilibrium phenomena, J. Phys. Soc. Jpn. **92**, 072001 (2023).